Received: 14 October 2021 | Revised: 18 February 2022 | Accepted: 9 March 2022

DOI: 10.1111/cas.15330

Cancer Science WILEY

ORIGINAL ARTICLE

Bone morphogenetic protein receptor 1α promotes osteolytic lesion of oral squamous cell carcinoma by SHH-dependent osteoclastogenesis

Qiao Qiao[1,2,3,4] | Le Xu[1,2,3,4,5] | Qingxiang Li[1,2,3,4] | Yifei Wang[1,2,3,4] | Han Lu[1,2,3,4,6] | Ning Zhao[1,2,3,4] | Yinfei Pu[1,2,3,4,7] | Lin Wang[1,2,3,4] | Yuxing Guo[1,2,3,4] | Chuanbin Guo[1,2,3,4]

[1]Department of Oral and Maxillofacial Surgery, Peking University School and Hospital of Stomatology, Beijing, China

[2]National Clinical Research Center for Oral Diseases, Beijing, China

[3]National Engineering Laboratory for Digital and Material Technology of Stomatology, Beijing, China

[4]Beijing Key Laboratory of Digital Stomatology, Peking University School and Hospital of Stomatology, Beijing, China

[5]Department of Oral and Maxillofacial Surgery, Shandong Provincial Hospital Affiliated to Shandong First Medical University, Shandong, China

[6]Shanghai Stomotological Hospital, Fudan University, Shanghai, China

[7]The Second Outpatient Department, Peking University School and Hospital of Stomatology, Beijing, China

Correspondence
Yuxing Guo and Chuanbin Guo, Department of Oral and Maxillofacial Surgery, Peking University School and Hospital of Stomatology, No. 22, Zhongguancun South Street, Haidian District, Beijing 100081, China.
Emails: gladiater1984@163.com (Y. G.); guodazuo@sina.com (C. G.)

Funding information
Beijing Municipal Natural Science Foundation, Grant/Award Number: 7212137; Program of The National Natural Science Foundation of China, Grant/Award Number: 81672664, 81900979, and 81972540; Peking University Medical Youth Science and Technology Innovation Foundation, Grant/Award Number: BMU2018PY004

Abstract

Oral squamous cell carcinoma (OSCC) is an aggressive tumor that usually invades the maxilla or mandible. The extent and pattern of mandibular bone invasion caused by OSCC are the most important factors determining the treatment plan and patients' prognosis. Yet, the process of mandibular invasion is not fully understood. The following study explores the molecular mechanism that regulates the mandibular invasion of OSCC by focusing on bone morphogenetic protein receptor 1α (BMPR1α) and Sonic hedgehog (SHH) signals. We found that BMPR1α was positively correlated to bone defect of OSCC patients. Mechanistically, BMPR1α signaling regulated the differentiation and resorption activity of osteoclasts through the interaction of OSCC cells and osteoclast progenitors, and this process was mediated by SHH secreted by tumor cells. The inhibition of SHH protected bone from tumor-induced osteolytic activity. These results provide a potential new treatment strategy for controlling OSCC from invading the jawbones.

Abbreviations: BMM, bone marrow-derived macrophage; BMP, bone morphogenetic protein; BMPR1α, bone morphogenetic protein receptor 1α; BV, bone volume; CT, computed tomography; HNSCC, head and neck squamous cell carcinoma; hpf, high-power field; IHC, immunohistochemistry; IHH, Indian hedgehog; IL-6, interleukin-6; M-CSF, macrophage colony-stimulating factor; NC, negative control; OSCC, oral squamous cell carcinoma; PTHrP, parathyroid hormone-related protein; RANKL, receptor activator of nuclear factor-κB ligand; SHH, Sonic hedgehog; TBME, tumor-bone microenvironment; TRAP, tartrate-resistant acid phosphatase; TV, total volume.

Qiao Qiao and Le Xu contributed equally to this study.

KEYWORDS
bone invasion, bone morphogenetic protein receptor 1α, hedgehog pathway, oral squamous cell carcinoma, tumor-bone microenvironment

1 | INTRODUCTION

Oral squamous cell carcinoma, which accounts for approximately 40% of all HNSCC, is an aggressive type of tumor associated with high mortality and a low response to chemotherapy.[1] The predilection sites of OSCC are the tongue and gingiva, through which OSCC invades the maxillary or mandibular bone.[2] Therefore, the extent and pattern of mandibular bone invasion caused by OSCC are the most important factors for determining the treatment plan and patients' prognosis.[3]

The osteolytic destruction caused by osteoclasts and proteolytic enzymes is often the result of bone invasion by cancer cells. This process requires the cell-cell interaction in the TBME, which affects tumorigenesis, progression, and treatment response.[1] Osteoclasts derived from hematopoietic stem cells are the main effector cells responsible for bone resorption. After being recruited into the bone resorption site, hematopoietic stem cells differentiate into osteoclasts through RANKL/RANK/OPG signaling, which then secrete collagenases, matrix metalloproteinases, and other enzymes, destroying and reabsorbing mineral substances of bone, and finally resulting in loss of bone tissues.

Tumor cells usually secrete various factors that affect the bone resorption function of adjacent osteoclasts. It is believed that a potential control of those factors could regulate osteoclast generation, differentiation, and function and, in turn, constrain bone invasion or metastasis. The BMP family is widely involved in the formation, growth, and metastasis of HNSCC.[4–7] Bone morphogenetic protein receptor 1α is one of the most important receptors mediating BMP signaling; yet, its role in tumor progression is not fully understood. Moreover, Cannonier et al discovered that hedgehog signaling has an important role during the OSCC invasion into the mandible.[8] Sonic hedgehog, a known regulator of OSCC microenvironment, can activate the status of cancer-associated fibroblasts and strengthen the differentiation and bone invasion through osteoclasts.[9,10] However, the molecular mechanisms that control SHH expression in OSCC remain unclear.

In this study, we explored the molecular mechanism that regulates the mandibular invasion of OSCC by focusing on BMPR1α on SHH signals.

2 | MATERIAL AND METHODS

2.1 | Patients

The study was approved by the Biomedical Ethics Committee of Peking University School and Hospital of Stomatology (PKUSSIRB-202054061).

Patients diagnosed with lower gingival OSCC in Peking University School and Hospital of Stomatology between June 2013 and December 2015 were enrolled in this study. The inclusion criteria were: (a) patients with detailed clinical information; (b) those who underwent CT; (c) lower gingival OSCC confirmed by pathological diagnosis; and (d) patients older than 18 years of age. The exclusion criteria were: (a) patients with incomplete clinical data or follow-up information; and (b) patients with immune system disorders. The diagnostic criteria were based on the TNM classification of malignant tumors[11] and WHO classification of head and neck tumors.[12]

2.2 | Animals

BALB/c male nude mice, 4-6 weeks old, weighing 20-25 g, were obtained from Vital River Laboratory Animal Technology. All the animals were housed in an environment with a temperature of 22 ± 1°C, relative humidity of 50 ± 1%, and a light / dark cycle of 12/12 hours. All animal studies (including the mice euthanasia procedure) were done in compliance with Peking University institutional animal care regulations and guidelines and conducted carried out to the AAALAC and IACUC guidelines (2020/06/19, No. LA2020378).

2.3 | Anteromedial tibia tumor mouse model and tumor growth estimation

An anteromedial tibia tumor model was established to investigate the bone invasion of tumor cells in vivo. Control (sh-NC) or sh-BMPR1α WSU-HN6 cells were resuspended with a concentration of 10^6 cells/100 μL. Then, 100 μL cell suspension was injected into the anteromedial tibia of BALB/c nude mice (Vital River Laboratory Animal Technology). Mice were subjected to further analysis after 3 weeks. GDC-0449 (20 mg/kg, Selleck Chemicals) was used to inhibit SHH, while SAG (25 mg/kg; Sigma-Aldrich) was used as the agonist of SHH; both substances were injected intraperitoneally when the tumor volume reached approximately 100 mm^3, followed by injection every 3 days. After 2 weeks, mice were killed, and the tissue was collected and analyzed ex vivo.[13]

Fluorescence from the GFP-conjugated lentiviral vector was measured by IVIS Lumina III (PerkinElmer). The radiant efficiency was analyzed by Living Image. The tumor volume was calculated using the following equation[14]: $V = 0.2618 \times L \times W \times (L + W)$, where W is the average distance in the proximal tibia at the level of the knee joint in the anterior-posterior and medial-lateral planes, and L is the distance from the edge of the proximal of the tumor to the distal extent of the tumor.

2.4 | Immunohistochemistry and immunofluorescence

Samples were blocked with 10% goat serum and incubated with the Ab at 4°C overnight. SPlink Detection Kits (ZSGB-BIO) were used for IHC according to the manufacturer's instructions. The slides were observed and photographed with an Olympus microscope, and the images were analyzed by ImageJ to measure the percentage of the positive zone. Five random fields were selected for analysis.

For F-actin rings observation, cells were fixed with 4% paraformaldehyde, blocked with 10% goat serum, and incubated with rhodamine-phalloidin (1:200, PHDR1; Sigma-Aldrich) for 15 minutes. Next, the slides were mounted with a mounting medium and stained with DAPI (ZSGB-BIO), after which the at least five random fields were photographed with an inverted phase-contrast (fluorescence) microscope (Olympus).

2.5 | Tartrate-resistant acid phosphatase staining

A TRAP staining kit (387A; Sigma-Aldrich) was used to detect $TRAP^+$ osteoclasts according to the manufacturer's instructions. To evaluate the osteoclast formation ability in vitro, a total number of $TRAP^+$ cells per hpf and the percentage of $TRAP^+$ area of five randomly selected fields were analyzed using ImageJ software.

2.6 | Computerized tomography and micro-CT

Computed tomography data of OSCC patients were collected, and the proportion of bone defects (mandible) was calculated. Briefly, a 3D reconstruction was performed, and the volume difference (H − A) between the healthy side (H) and the affected side (A) of the mandible was calculated using the following formula: $(H - A)/2H$, representing the bone defect proportion. For cases with tumors involving both sides of the mandible, the healthy mandible was replenished according to the natural anatomy. The whole process was undertaken using iPlan Navigator (Brainlab).

For analyzing the bone defect of the mouse tibia, anteromedial tibias of mice were scanned by micro-CT (Inveon MM Gantry-STD) with a 9 μm resolution ratio (60 kVp, 220 μA). Inveon Research Workplace (Siemens) was used to reconstruct a 3D image of the tibia. The ratio of BV to TV was used to assess bone loss.

2.7 | Bone marrow-derived macrophages and osteoclast formation

To induce osteoclast differentiation, BMMs were cultured with medium supplemented with 50 ng/mL M-CSF (R&D Systems) for 3 days (stage I), followed by 50 ng/mL RANKL (R&D Systems) and 50 ng/mL M-CSF stimulation for another 5 days (stage II). The conditioned medium from sh-NC and sh-BMPR1α WSU-HN6 cells were added at stage II to mimic the in vivo TBME. To examine the effect of SHH, rm-SHH (50 ng/mL; R&D Systems) or GDC-0449 (500 ng/mL) were added at stage II. The cells were then fixed or collected for further analysis.

2.8 | Bone resorption assay

A bone resorption assay was carried out to detect the resorption activity of osteoclasts. Bone marrow cells were plated in 24-well osteo assay plates (Corning osteo assay, CLS3987; Sigma-Aldrich) and cultured with the aforementioned conditional medium or reagents. After 10 days, the plates were observed using an Olympus microscope and analyzed by ImageJ to calculate the resorbed area.

2.9 | Statistical analysis

SPSS 26.0 (IBM) was used for statistical analysis. Student's *t* test was used to analyze the data between two groups; Tukey's test was used to analyze data among multiple groups. Survival time was compared using the log-rank test, and Kaplan-Meier was used to calculate the accumulated survival rate. The correlation test was analyzed by the Pearson test. $P < .05$ was considered statistically significant.

More information on detailed materials and methods is available in Appendix S1.

3 | RESULTS

3.1 | Expression of BMPR1α positively correlated with bone invasion in human OSCC

First, we examined the expression of BMP family receptors in specimens collected from patients with lower gingival OSCC (Figure 1A). *ACVR2B*, *BMPR2*, *ALK1*, *and ALK2* were upregulated in OSCC tissue compared with paracarcinoma tissue, although without statistical significance. Among the seven receptors, *BMPR1α and BMPR1β* showed a significant increase in OSCC tissue, and *BMPR1α* expression level was higher than *BMPR1β*.

Next, the basic information of 104 cases diagnosed with lower gingival OSCC was collected, and the location and extent of jaw bone invasion were analyzed. The lesions that occurred behind the mental foramen of the mandible accounted for the vast majority of cases (88/104; Table 1).

Seventy-seven of the cases with well-stored pathological specimens were included for further analysis. Immunohistochemical analysis of BMPR1α was carried out to estimate the expression of BMPR1α (Figure 1B). Moreover, the bone defect volume of the

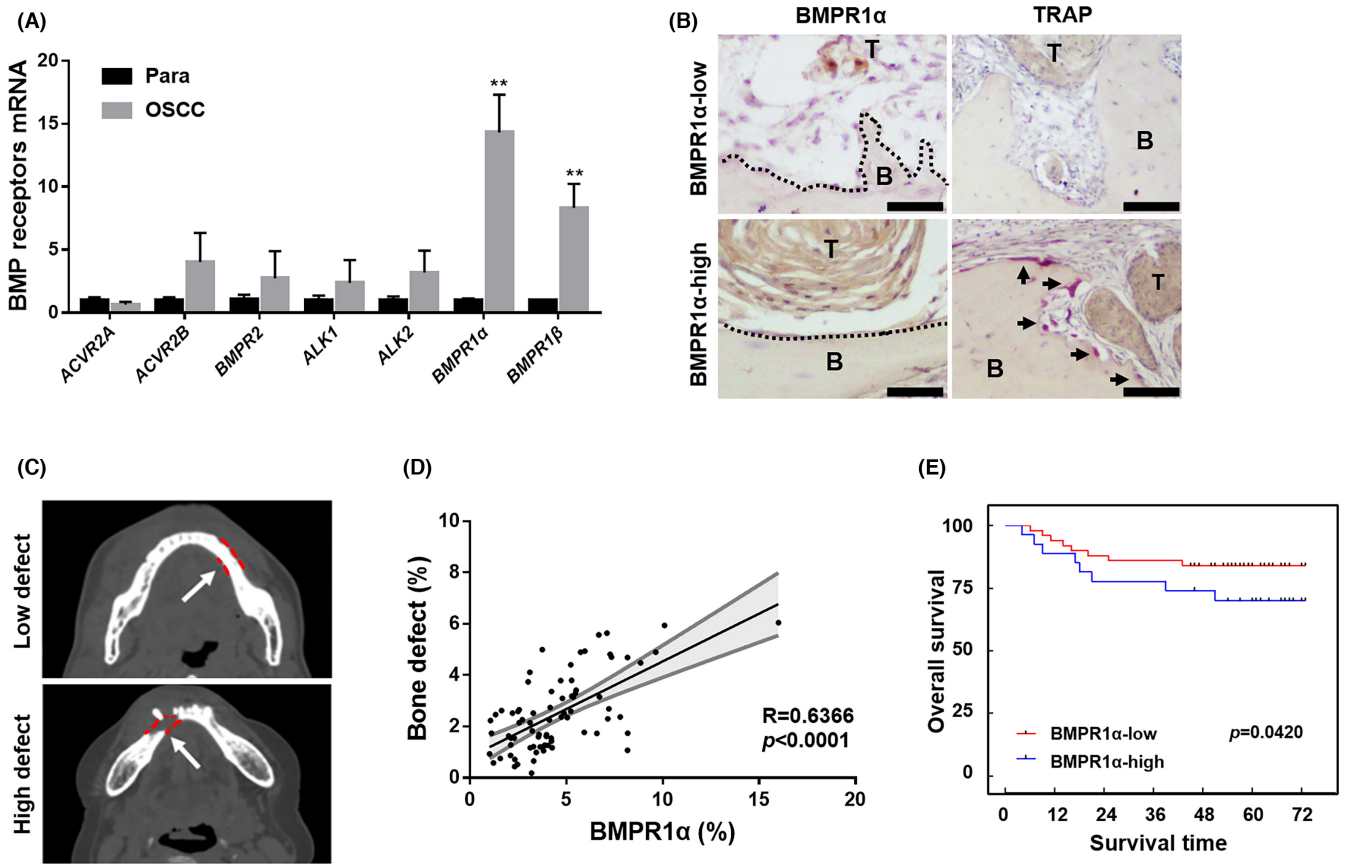

FIGURE 1 Bone morphogenetic protein receptor 1α (BMPR1α) level positively correlates with increased bone invasion in human oral squamous cell carcinoma (OSCC). (A) Quantitative RT-PCR was performed to examine the receptors of the bone morphogenetic protein (BMP) family in tumor and paratumor tissues from patients with lower gingival OSCC. $n = 6$. (B) Immunohistochemical staining of BMPR1α (left) was used to estimate the expression of BMPR1α in tumor tissue. Tartrate-resistant acid phosphatase (TRAP) staining (right) was used to indicate osteoclasts (arrows) at the tumor (T)-bone (B) interface (dotted line). Scale bar, 50 μm. (C, D) Representative computed tomography axial images of the mandible of patients with OSCC. The proportion of bone defects (total bone volume) caused by tumor invasion was calculated. Correlation analysis was used to explore the relation between BMPR1α expression level and bone defect proportion. $n = 77$. Dotted line, outline of mandible; white arrow, bone defect site. (E) Cumulative survival rate and survival time of OSCC cases with high and low BMPR1α expression. $n = 77$. $^{*}P < .05$, $^{**}P < .01$

above patients' mandible and the proportion of bone defects caused by tumor invasion were calculated (Figure 1C). The correlation analysis results showed that BMPR1α expression level was positively correlated with proportion of bone defects invaded by OSCC (Figure 1D). In addition, a larger number of $TRAP^{+}$ osteoclasts was observed in the tumor-bone invasion site with high expression of BMPR1α (Figure 1B).

Furthermore, survival analysis revealed that the prognosis of OSCC cases in the BMPR1α-high expression group was worse than the BMPR1α-low expression group (Figure 1E).

3.2 | Bone morphogenetic protein receptor 1α participates in bone invasion by regulating the differentiation of osteoclasts

To explore the tumor biological role of BMPR1α, we collected the cDNA of four OSCC cell lines (WSU-HN6, SCC15, SCC25, and CAL27) and performed quantitative RT-PCR. As shown in Figure 2A, the expression of the BMPR1α gene was higher in WSU-HN6 cells and CAL27 cells compared to other cells. Thus, WSU-HN6 cells, which expressed the highest levels of the *BMPR1α* gene, were selected for further experiments. Then GFP-conjugated BMPR1α shRNA or sh-NC was transfected into WSU-HN6 cells by a lentiviral vector, and the knockdown efficacy was verified by quantitative RT-PCR and western blot analysis (Figure S1).

In order to better quantify the extent of bone invasion, an anteromedial tibia tumor cell implantation model was established using sh-NC and sh-BMPR1α WSU-HN6 cells. Three weeks later, the mice were killed to analyze the extent of bone destruction caused by the tumor (Figure 2B). The significantly decreased radiant efficiency in the BMPR1α knockdown mice compared with non-BMPR1α knockdown mice implied that the reduced tumor burden was caused by the knockdown of BMPR1α (Figure 2C,D). Furthermore, micro-CT data showed that mice implanted with sh-NC tumor cells suffered a

TABLE 1 Overview of 104 patients with lower gingival oral squamous cell carcinoma

Clinical information	Case number (%)
Sex	
Male	57 (54.8)
Female	47 (45.2)
Age, y	
≤65	66 (63.5)
>65	38 (36.5)
T stage	
T1	17 (16.3)
T2	30 (28.8)
T3	4 (3.8)
T4	53 (51.0)
N stage	
N0	70 (67.3)
N1	16 (15.4)
N2	18 (17.3)
M stage	
M0	104 (100.0)
M1	0 (0.0)
Pathological grade	
I	48 (46.2)
II	51 (49.0)
III	5 (4.8)
Primary site	
Anterior mandibular	16 (15.4)
Posterior mandibular	88 (84.6)
Depth of bone invasion	
None	18 (17.3)
Cortical bone	33 (31.7)
Marrow	33 (31.7)
Mandibular canal	20 (19.3)
Local recurrence	
Negative	70 (67.3)
Positive	34 (32.7)

stronger bone invasion (involving the tibia; Figure 2C) and had lower BV/TV compared to mice injected with sh-BMPR1α WSU-HN6 cells (Figure 2C,E). At the same time, fewer TRAP$^+$ cells were seen at the tibia-tumor junction in the BMPR1α knockdown group mice than in the control group (Figure 2C,F). In addition, the HN6 cells showed the strongest bone resorption ability compared to other OSCC cells (Figure S2).

Receptor activator of nuclear factor κ-B ligand is critical for bone invasion and is responsible for the differentiation of osteoclast differentiation.[15] In the tumor tissues of mice injected with BMPR1α knockdown tumor cells, the expression of RANKL was significantly decreased, as shown by IHC (Figure 2C,G).

3.3 | Expression of BMPR1α in OSCC tumor cells affects the differentiation and resorption function of osteoclasts

The culture supernatants from sh-NC and sh-BMPR1α WSU-HN6 cells were used as the conditioned medium to further verify the role of BMPR1α expression level in OSCC on the differentiation of osteoclasts. The TRAP staining results showed significantly decreased osteoclast differentiation in the sh-BMPR1α medium compared to the sh-NC medium, as confirmed by the osteoclast number and percentage of TRAP$^+$ area per hpf (Figure 3A-C).

Previous study reported that the formation of F-actin rings is required for the resorption function of osteoclasts.[16] The organized, sharply defined structures of F-actin rings, such as ruffled borders and sealing zone represent normal function of osteoclasts,[17,18] and this process is related with the osteoclast-related genes including *NFATc1*, *ATP6v0d2*, and *RANKL*.[19,20] Immunofluorescence staining showed that osteoclasts with OSCC cell-derived conditioned medium formed organized F-actin rings, whereas disorganized F-actin rings were found in groups induced with conditioned medium from BMPR1α knockdown OSCC cells (Figure 3A). Thus, we speculated that the resorption function was weakened in the conditioned medium obtained from BMPR1α knockdown OSCC cells, as confirmed by bone resorption assay (Figure 3A,D). Meanwhile, the mRNA levels of osteoclastogenic markers, such as *rankl*, *nfatc1*, *cathepsin k*, and *atp6v0d2*, were all decreased in the sh-BMPR1α WSU-HN6 group compared to the sh-NC group (Figure 3E). To sum up, we concluded that the expression level of the *BMPR1α* gene in tumor cells might participate in bone invasion by regulating osteoclast differentiation.

3.4 | Bone morphogenetic protein receptor 1α regulates the expression of SHH in tumor cells of OSCC

Previous studies reported that hedgehog signaling might participate in BMP-induced signaling of mesenchymal stem cells and cancer cell activities.[21–23] In addition, our previous study found that IHH has a critical role in calvarial bone homeostasis and repair through regulation of osteoclast differentiation.[24] Thus, we hypothesized that BMPR1α-related bone invasion might be hedgehog signaling-dependent. Thus, we analyzed the expression of the hedgehog family, including IHH, SHH, and Desert hedgehog in sh-NC and sh-BMPR1α WSU-HN6 cells. Bone morphogenetic protein receptor 1α knockdown or inhibition by BMP signaling significantly decreased the expression of *SHH* in WSU-HN6 cells (Figures 4A and S3A). Western blot results further confirmed decreased SHH expression after BMPR1α was decreased (Figure 4B).

Through in silico promoter analysis, we found potential sequences at the promoter of SHH that might be binding sequences of Smad4, the downstream transcription factor of BMP signaling (Figure S3B). Next, the ChIP assay confirmed the binding of Smad4 with SHH promoter in tumor cells (Figure 4C). After BMPR1α was inhibited, the ChIP results indicated a reduction of Smad4 occupied on the promoter of *SHH* (Figures 4C and S3C). Accordingly, the

Smad1/5/8 pathway, downstream of BMP signaling, was also decreased in sh-BMPR1α cells or in the LND-193189 (BMP signaling inhibitor) group (Figure 4D), resulting in the decreased expression and secretion of SHH (Figure S3D,E).

To verify the relation of BMPR1α and SHH, specimens of the aforementioned cases were subjected to IHC staining. The results verified the positive correlation of SHH with BMPR1α in OSCC tissue (Figure 4E,F).

3.5 | Sonic hedgehog mediates BMPR1α-induced osteoclast differentiation

Next, we examined whether BMPR1α-induced osteoclast differentiation is regulated in an SHH-dependent manner. We induced BMM with sh-NC or sh-BMPR1α medium and treated sh-BMPR1α group cells with recombined mouse SHH to upregulate the hedgehog signaling. Staining with TRAP showed that the osteoclast number

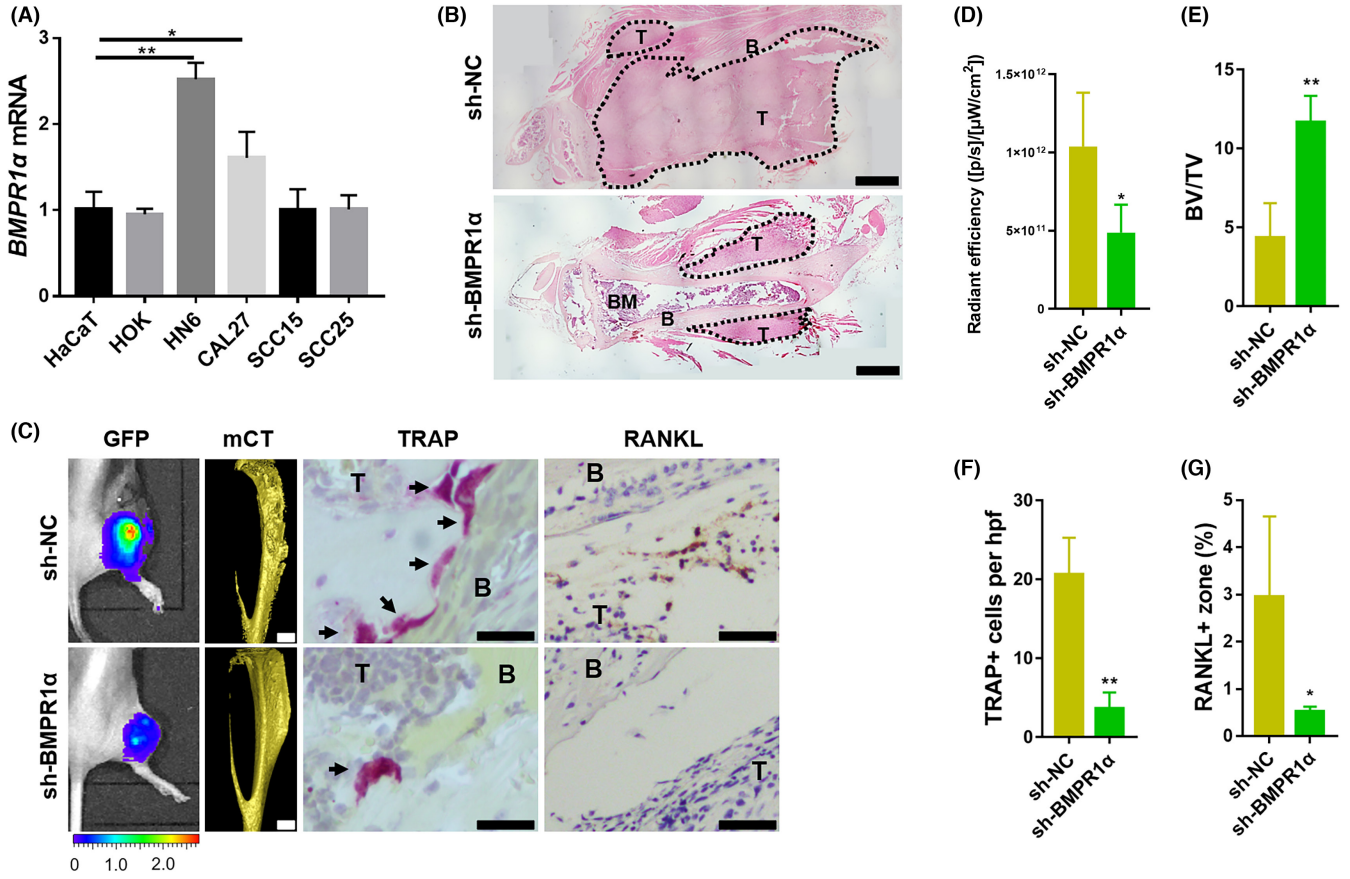

FIGURE 2 Bone morphogenetic protein receptor 1α (BMPR1α) participates in bone invasion by regulating the differentiation of osteoclasts in mice. (A) Quantitative RT-PCR was used to evaluate the expression of the BMPR family in four head and neck squamous cell carcinoma (SCC) cell lines. HaCaT cells were used as control. $n = 3$ for every cell line. (B) GFP-conjugated BMPR1α shRNA was transferred into WSU-HN6 cells by a lentiviral vector. An anteromedial tibia tumor cell implantation mouse model was established. Representative images of H&E staining showing tumor burden and bone defect. Dotted line shows tumor-bone interface. Scale bar, 1 mm. (C) Representative images of fluorescence imaging, 3D micro-CT (mCT) reconstruction, tartrate-resistant acid phosphatase (TRAP) staining, and receptor activator of nuclear factor-κB ligand (RANKL) immunohistochemical staining of mouse tibia implanted with normal control (sh-NC) and sh-BMPR1α WSU-HN6 cell lines for 3 weeks. Black arrows indicate osteoclasts. Scale bars, 1 mm for mCT, 50 μm for TRAP and RANKL staining. $n = 5$. (D-G) Radiant efficiency of fluorescence imaging (D), statistical results of bone volume fraction (bone volume [BV]/total volume [TV]) (E), TRAP$^+$ osteoclast number under 10× high magnification per view (F), and RANKL$^+$ zone per view (G) ($n = 5$). $^*P < .05$, $^{**}P < .01$. B, bone; BM, bone marrow; T, tumor

FIGURE 3 Bone morphogenetic protein receptor 1α (BMPR1α) expression in oral squamous cell carcinoma tumor cells affects the differentiation and resorption function of osteoclasts. (A) Bone marrow-derived macrophages (BMMs) were divided and cultured with control medium (DMEM) or conditional medium from normal control (sh-NC) and sh-BMPR1α WSU-HN6 culture supernatants. BMMs were induced with receptor activator of nuclear factor-κB ligand (RANKL) for 5 days. Representative images of tartrate-resistant acid phosphatase (TRAP) staining, F-actin immunofluorescence staining, and bone resorption assay of BMM induced by conditioned medium. Scale bar, 200 μm. (B, C) Quantitation of osteoclast number (B) and percentage of TRAP$^+$ area (C) per high-power field (hpf) in TRAP staining assay ($n = 3$). (D) Quantitation of total resorption area per hpf in the resorption activity assay. ($n = 3$). (E) Quantitative RT-PCR was used to evaluate the expression of *rankl*, *nfatc1*, *cathepsin k*, and *atp6v0d2* of BMM with conditioned medium obtained from sh-NC and sh-BMPR1α WSU-HN6 cells ($n = 3$). $^*P < .05$, $^{**}P < .01$

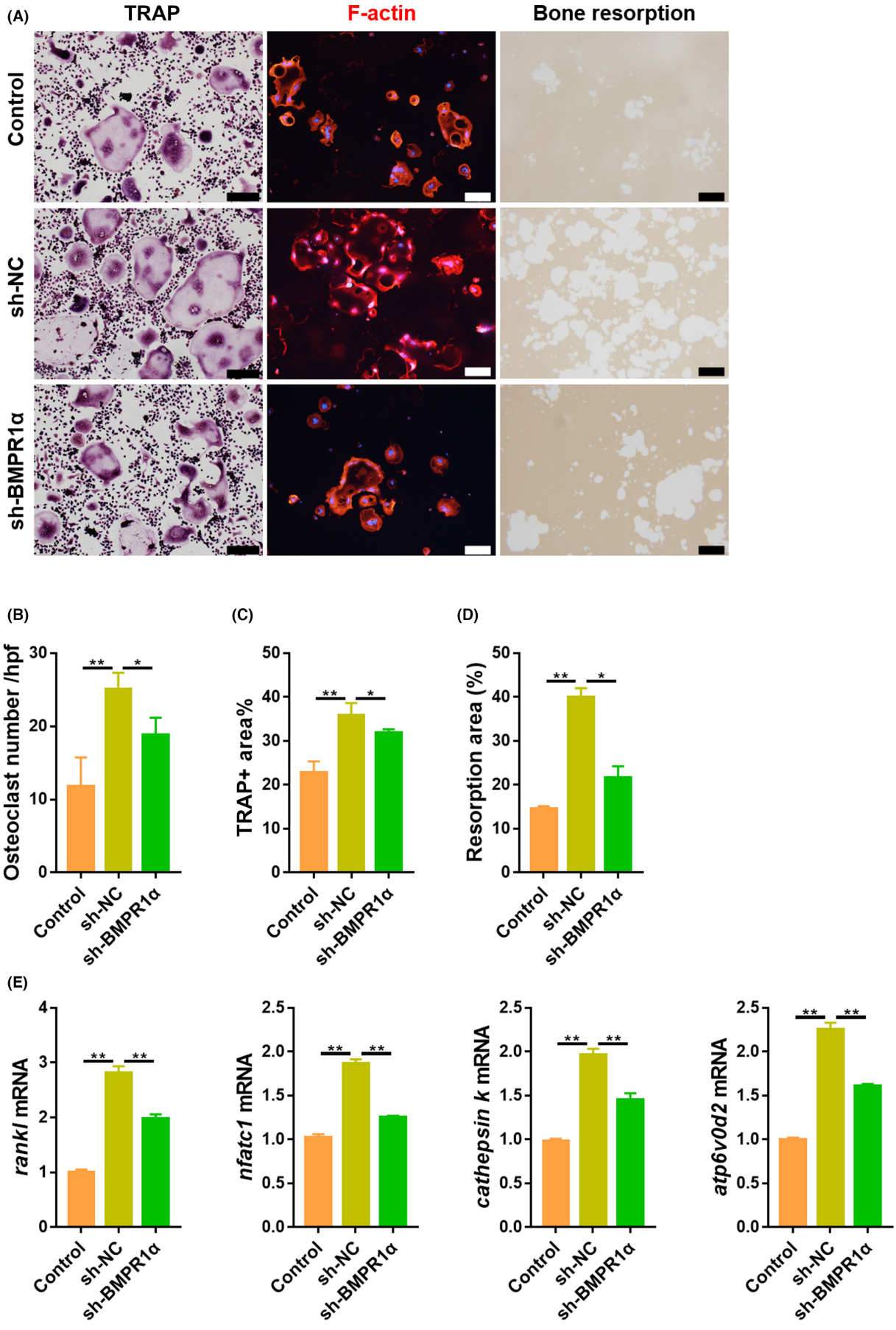
(A)
TRAP
F-actin
Bone resorption
Control
sh-NC
sh-BMPR1α
(B)
Osteoclast number /hpf
(C)
TRAP+ area%
(D)
Resorption area (%)
(E)
rankl mRNA
nfatc1 mRNA
cathepsin k mRNA
atp6v0d2 mRNA
Control
sh-NC
sh-BMPR1α

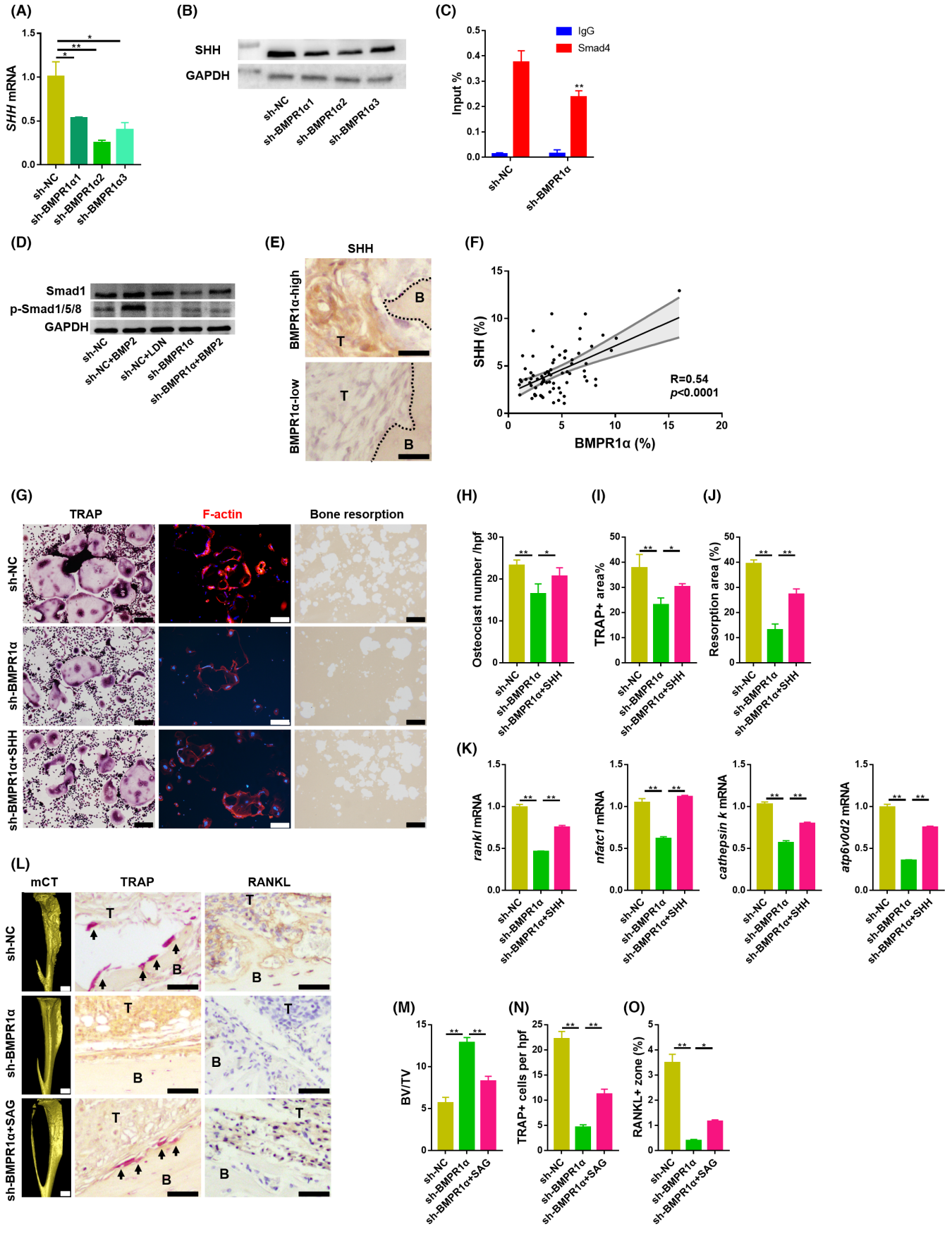
(A)
SHH mRNA
sh-NC
sh-BMPR1α1
sh-BMPR1α2
sh-BMPR1α3
(B)
SHH
GAPDH
(C)
IgG
Smad4
Input %
(D)
Smad1
p-Smad1/5/8
GAPDH
sh-NC+BMP2
sh-NC+LDN
sh-BMPR1α
sh-BMPR1α+BMP2
(E)
SHH
BMPR1α-high
BMPR1α-low
(F)
SHH (%)
BMPR1α (%)
R=0.54
p<0.0001
(G)
TRAP
F-actin
Bone resorption
sh-BMPR1α+SHH
(H)
Osteoclast number /hpf
(I)
TRAP+ area%
(J)
Resorption area (%)
(K)
rankl mRNA
nfatc1 mRNA
cathepsin k mRNA
atp6v0d2 mRNA
(L)
mCT
RANKL
sh-BMPR1α+SAG
(M)
BV/TV
(N)
TRAP+ cells per hpf
(O)
RANKL+ zone (%)

FIGURE 4 Sonic hedgehog (SHH) mediates bone morphogenetic protein receptor 1α (BMPR1α)-induced osteoclast differentiation. (A) Quantitative RT-PCR was used to detect the mRNA levels of *SHH* after BMPR1α knockdown ($n = 3$). (B) Western blot was used to detect SHH protein levels after BMPR1α knockdown ($n = 3$). (C) ChIP assay was used to demonstrate the direct binding of Smad4 with the SHH promoter and to verify the occupying of Smad4 on the promoter of *SHH* after BMPR1α knockdown ($n = 3$). (D) Western blot was used to detect the phosphorylation levels of Smad1/5/8 ($n = 3$). (E) Representative images of SHH immunohistochemical (IHC) staining in tissues from BMPR1α low and high expression cases. Dotted line indicates bone (B)-tumor (T) interface. Scale bar, 50 μm. (F) Correlation analysis was performed to explore the relation between BMPR1α and SHH expression in selected low gingival oral squamous cell carcinoma cases ($n = 77$). (G) Bone marrow-derived macrophages (BMMs) were divided and cultured with normal control (sh-NC) or sh-BMPR1α WSU-HN6 culture supernatants as the conditioned medium. BMM was then induced with receptor activator of nuclear factor-κB ligand (RANKL) for 5 days. For the recovery of SHH stimulation, 50 ng/mL rm-SHH was added with RANKL. Representative images of tartrate-resistant acid phosphatase (TRAP) staining, F-actin immunofluorescence staining, and bone resorption assay of BMMs induced by conditioned medium. Scale bar, 200 μm. (H, I) Quantitation of osteoclast number (H) and percentage of $TRAP^+$ area (I) per high-power field (hpf) in TRAP staining assay ($n = 3$). (J) Quantitation of total resorption area per hpf in the resorption activity assay ($n = 3$). (K) Quantitative RT-PCR was used to evaluate the expression of *rankl*, *nfatc1*, *cathepsin k*, and *atp6v0d2* of BMM with conditioned medium obtained from sh-NC and sh-BMPR1α WSU-HN6 cells ($n = 3$). (L) An anteromedial tibia tumor cell implantation mouse model was established with sh-NC, sh- BMPR1α, and sh-BMPR1α plus SHH agonist SAG. Representative images of 3D micro-computed tomography (mCT) reconstruction, TRAP staining, and RANKL IHC staining of mouse tibia implanted with tumor cell lines. Black arrows indicate osteoclasts. B, bone; T, tumor. Scale bars, 1 mm for mCT, 50 μm for TRAP and RANKL staining. $n = 5$. (M-O) Statistical results of bone volume (BV)/total volume (TV) (M), $TRAP^+$ osteoclast number under 10× high magnification per view (N), and $RANKL^+$ zone per view (O) are shown ($n = 5$).$^*P < .05$, $^{**}P < .01$

and $TRAP^+$ area were resumed after SHH stimulation (Figure 4G-I). Immunofluorescence staining showed the F-actin rings with more organized structure, and bone resorption assay also confirmed recovered bone resorption ability after SHH stimulation in the sh-BMPR1α group (Figure 4G,J). In addition, the mRNA levels of *rankl*, *nfatc1*, *cathepsin k*, and *atp6v0d2* were restored (Figure 4K).

Next, an in vivo experiment was undertaken to verify whether SHH mediates BMPR1α-induced osteolytic lesion. Sonic hedgehog agonist SAG, which helps activate hedgehog signaling, was administrated. The 3D reconstruction of mouse tibia indicated that SAG treatment prevented the bone preservation effect of BMPR1α knockdown (Figure 4L,M). The TRAP staining verified recovered osteoclast numbers after SAG administration (Figure 4L,N). Immunohistochemistry also confirmed that RANKL was recovered under SAG stimulation (Figure 4L,O). In addition, SHH stimulation directly increased the expression of related mRNA, $TRAP^+$ osteoclasts, F-actin ring formation, and bone resorption capacity of osteoclasts (Figure S4).

3.6 | Hedgehog inhibition protects bone tissue from BMPR1α-induced osteolytic lesion

Next, we used GDC-0449, an inhibitor of hedgehog signaling targeting SMO, to test the potential therapeutic effect of SHH inhibition.[25] GDC-0449 weakened the enhanced osteoclast differentiation, F-actin ring formation, and resorption ability induced by the conditioned medium (Figure 5A-D). In addition, the expression of osteoclast-related genes was also decreased in the hedgehog inhibition group compared to the conditioned medium group (Figure 5E).

Next, the anteromedial tibia tumor cell implantation model was used to verify the effect of hedgehog inhibition on tumor-related osteolytic lesions. After treatment with GDC-0449, the tumor volume decreased (Figure 5F,G). Furthermore, the 3D reconstruction of mouse tibia showed that the bone loss induced by tumor invasion was significantly ameliorated by hedgehog inhibition (Figure 5H,I). Meanwhile, decreased osteoclast numbers were observed in the GDC-0449 group (Figure 5H,J). In addition, IHC confirmed decreased RANKL levels in the tumor area (Figure 5H,K). Therefore, our results prove that BMPR1α promotes osteolytic lesion of OSCC by SHH-dependent osteoclastogenesis (Figure 6) and has a therapeutic effect on OSCC-induced bone defect by inhibiting hedgehog signaling.

4 | DISCUSSION

Our data suggested that BMPR1α expression was positively correlated with OSCC tumor progression and mandibular invasion. Furthermore, we discovered that BMPR1α expression drove osteoclast differentiation to promote bone invasion of OSCC in an SHH signaling-dependent manner, whereas targeting SHH or BMPR1α protected the bone from tumor invasion. These findings suggest an important role of BMPR1α and SHH signaling in osteoclast differentiation and OSCC-induced osteolytic destruction, thus providing a potential strategy for molecular-targeted treatment.

Oral squamous cell carcinoma is an aggressive tumor associated with poor prognosis.[26–28] The cross-talk between cancer cells and bone cells (osteoblasts and osteoclasts) favors the proliferation of the tumor cells in the bone environment but also ultimately completes the subjugation of resident (bone) pathways that serve the purpose of establishment and well-being of the tumor cells with concurrent destruction of the bone structure.[29] Tumor-derived factors, such as IL-6 and PTHrP, induce RANKL expression on osteoblasts, leading to osteoclastogenesis.[28] Furthermore, the effectiveness of osteoblasts in the microenvironment increases the expression of osteopontin in oral cancer tumor cells, which in turn promotes the bone resorption function of osteoclasts.[30] Squamous cell carcinoma cells can directly enhance osteoclastogenesis by secreting RANKL, IL-6, CXCL12

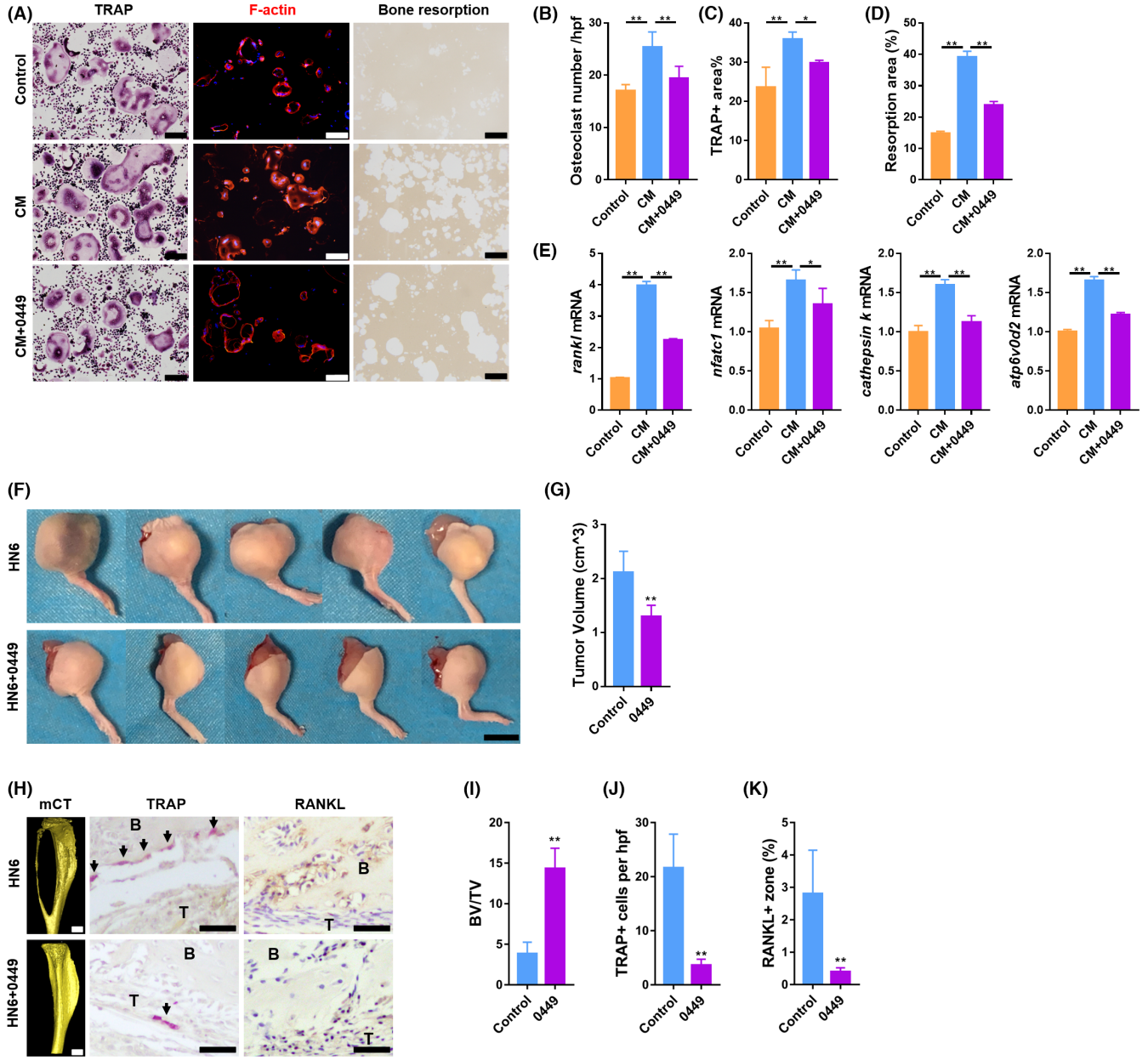

FIGURE 5 Hedgehog inhibition protects bone tissue from bone morphogenetic protein receptor 1α (BMPR1α)-induced osteolytic lesions. (A) Bone marrow-derived macrophages (BMMs) were divided and cultured with WSU-HN6 culture supernatants as the conditioned medium. BMMs were induced with receptor activator of nuclear factor-κB ligand (RANKL) for 5 days. For the inhibition of Sonic hedgehog (SHH) signaling, GDC-0449 was added to RANKL. Representative images of tartrate-resistant acid phosphatase (TRAP) staining, F-actin immunofluorescence staining, and bone resorption assay of BMM induced by conditioned medium. Scale bar, 200 μm. (B, C) Quantitation of osteoclast number (B) and percentage of $TRAP^+$ area (C) per high-power field (hpf) in TRAP staining assay $n = 3$. (D) Quantitation of total resorption area per hpf in the resorption activity assay $n = 3$. (E) Quantitative RT-PCR was used to evaluate the expression of *rankl*, *nfatc1*, *cathepsin k*, and *atp6v0d2* of BMM with conditioned medium obtained from normal control (sh-NC) and sh-BMPR1α WSU-HN6 cells ($n = 3$). (F) An anteromedial tibia tumor cell implantation mouse model was established with WSU-HN6 cells and WSU-HN6 cells plus GDC-0449. Images of the hind limb of mice where WSU-HN6 cells were injected. Scale bar, 1 cm. (G) Quantitation of the tumor volume of mice in each group ($n = 5$). (H) Representative images of 3D micro-computed tomography (mCT) reconstruction, TRAP staining, and RANKL immunohistochemical staining of mouse tibia implanted with tumor cell lines. Black arrows indicate osteoclasts. B, bone, T, tumor. Scale bars, 1 mm for mCT, 50 μm for TRAP and RANKL staining. $n = 5$. (I-K) Statistical results of bone volume (BV)/total volume (TV) (G), $TRAP^+$ osteoclast number per view (H), and $RANKL^+$ zone per view (I) are shown ($n = 5$). * $P < .05$, ** $P < .01$

(SDF-1), CXCL13, tumor necrosis factor-α, prostaglandin E2/F2, monocyte chemoattractant protein-1, and PTHrP.[31–39] Therefore, further understanding the interactions between tumor and bone cells and identifying microenvironment-selective agents to halt tumor growth and bone invasion, thus reducing destruction, is of crucial importance.

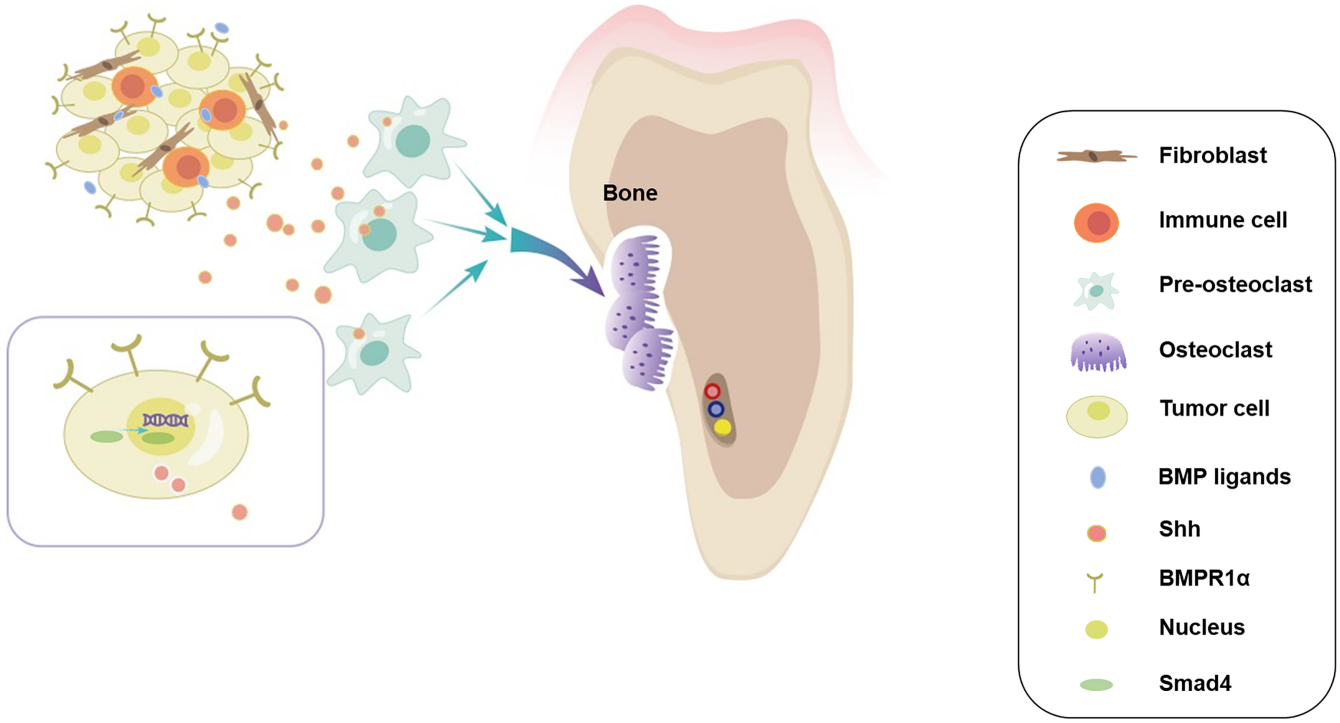

FIGURE 6 In oral squamous cell carcinoma (OSCC) tissues, overexpression of bone morphogenetic protein receptor 1α (BMPR1α) activates downstream signaling and induces expression of Sonic hedgehog (SHH) regulated by transcription factor Smad4. SHH enhances osteoclasts' differentiation and resorption activity in a paracrine way, promoting the bond defect induced by OSCC

The BMP family is the main growth factor with an important role in bone regeneration.[40] However, several studies have found that excessive BMP-2 could lead to tumor progression. Zhou et al[41] analyzed tongue squamous cell carcinoma samples by gene microarray and quantitative PCR and found that the expression level of BMP-2 was associated with lymph node metastasis. Furthermore, Kim et al suggested that rhBMP-2 promotes OSCC invasion by inducing CCL5 release[42]; thus, suggesting that a detailed clinical examination should be undertaken and that suspicious malignant tissues in adjacent areas should be treated or removed before the use of rhBMP-2-loaded biomaterials to eliminate adverse reactions caused by rhBMP-2.

Bone morphogenetic protein receptor 1α is one of the most important receptors mediating BMP-2 signaling; yet, its role in tumor progression is not fully understood. A study focusing on prostate cancer found that loss of myeloid BMPR1α restricted tumor progression in a syngeneic mouse prostate cancer model.[43] It was also shown that deletion of BMPR1α in colon cancer could sensitize cells to chemotherapy and that high *BMPR1α* gene expression was correlated with decreased survival regardless of molecular breast cancer subtype.[44,45] Using transcriptomic profiling of isolated bone lining cell subtypes from a murine myeloma model, Gooding et al found that solubilized BMPR1α-FC receptor-ligand trap could prevent trabecular and cortical bone volume loss caused by myeloma.[46] Factors secreted by tumor cells could interfere with bone homeostasis, reshaping the TBME. Moreover, previous studies have reported that SHH can help promote the activation of osteoclasts during malignant tumorigenesis.[10] A recent study reported that knockdown of PTCH1 can downregulate hedgehog signaling by inhibiting the smoothened activity in non-small-cell lung cancer, which, in turn, leads to decreased bone destruction and osteoclastogenesis.[47] Both BMP and SHH have been reported to promote osteoclastogenesis during tumorigenesis and bone metastasis.[29,44,45] Some studies also suggested that BMP-mediated SHH signaling positively regulates the bone metastasis of prostate cancer.[48]

Bone invasion is considered a later stage of a disease, and the surgical treatment at this point can destroy jaw function and cause aesthetic problems. In the approaching era of personalized medicine, the current treatment methods targeting bone invasion environments of OSCC are provided to the patient with limited consideration of the cancer cells' origin. Our new outlook suggests delivering individual tumor microenvironment treatments based on the expression level/activity/functionality of tumor-derived factors, rather than utilizing a commonly shared therapeutic umbrella approach, therefore providing targeted treatment in combination with surgical treatment. We also provided evidence that hedgehog inhibition might be used as a potential strategy for blocking BMPR1α-induced bone defect and tumor progression. The notion of "BMPR1α-SHH-associated bone remodeling" could be a step toward a specific personalized therapy for OSCC generating a different bone niche in patients afflicted with incurable bone invasion. In this study, however, we did not analyze the metastasis development related to the bone invasion. Thus, more research is needed to further investigate the relationship between BMPR1α and tumor metastasis.

ACKNOWLEDGMENTS

The authors thank the Central Laboratory of Peking University School and Hospital of Stomatology for all their support during this research. This research was supported by Beijing Municipal Natural Science Foundation (7212137), Program of The National Natural Science Foundation of China (81672664, 81900979, and 81972540), and Peking University Medical Youth Science and Technology Innovation Foundation (BMU2018PY004).

DISCLOSURE

The authors have no conflict of interest.

ORCID

Yuxing Guo https://orcid.org/0000-0003-3564-7173

REFERENCES

1. Park J, Zhang X, Lee SK, et al. CCL28-induced RARbeta expression inhibits oral squamous cell carcinoma bone invasion. *J Clin Invest*. 2019;129:5381-5399.
2. Farrow ES, Boulanger T, Wojcik T, Lemaire AS, Raoul G, Julieron M. Magnetic resonance imaging and computed tomography in the assessment of mandibular invasion by squamous cell carcinoma of the oral cavity. Influence on surgical management and post-operative course. *Rev Stomatol Chir Maxillofac Chir Orale*. 2016;117:311-321.
3. Sacks D, Baxter B, Campbell B, et al. Multisociety Consensus Quality improvement revised consensus statement for endovascular therapy of acute ischemic stroke. *Int J Stroke*. 2018;13:612-632.
4. Alarmo EL, Huhtala H, Korhonen T, et al. Bone morphogenetic protein 4 expression in multiple normal and tumor tissues reveals its importance beyond development. *Mod Pathol*. 2013;26:10-21.
5. Xu T, Yu CY, Sun JJ, et al. Bone morphogenetic protein-4-induced epithelial-mesenchymal transition and invasiveness through Smad1-mediated signal pathway in squamous cell carcinoma of the head and neck. *Arch Med Res*. 2011;42:128-137.
6. Sand JP, Kokorina NA, Zakharkin SO, Lewis JJ, Nussenbaum B. BMP-2 expression correlates with local failure in head and neck squamous cell carcinoma. *Otolaryngol Head Neck Surg*. 2014;150:245-250.
7. Yang WH, Lan HY, Tai SK, Yang MH. Repression of bone morphogenetic protein 4 by let-7i attenuates mesenchymal migration of head and neck cancer cells. *Biochem Biophys Res Commun*. 2013;433:24-30.
8. Cannonier SA, Gonzales CB, Ely K, Guelcher SA, Sterling JA. Hedgehog and TGFbeta signaling converge on Gli2 to control bony invasion and bone destruction in oral squamous cell carcinoma. *Oncotarget*. 2016;7:76062-76075.
9. Guimaraes V, Vidal M, de Faro VL, et al. Hedgehog pathway activation in oral squamous cell carcinoma: cancer-associated fibroblasts exhibit nuclear GLI-1 localization. *J Mol Histol*. 2020;51:675-684.
10. Shimo T, Matsumoto K, Takabatake K, et al. The role of sonic Hedgehog signaling in osteoclastogenesis and jaw bone destruction. *PLoS One*. 2016;11:e151731.
11. Huang SH, O'Sullivan B. Overview of the 8th edition TNM classification for head and neck cancer. *Curr Treat Options Oncol*. 2017;18:40.
12. Speight PM, Takata T. New tumour entities in the 4th edition of the World Health Organization Classification of Head and Neck tumours: odontogenic and maxillofacial bone tumours. *Virchows Arch*. 2018;472(3):331-339.
13. Wang Y, Li Q, Xu L, et al. Cancer stemness of CD10-positive cells regulated by Hedgehog pathway promotes the resistance to cisplatin in oral squamous cell carcinoma. *Oral Dis*. 2021;27:1403-1411.
14. Luu HH, Kang Q, Park JK, et al. An orthotopic model of human osteosarcoma growth and spontaneous pulmonary metastasis. *Clin Exp Metastasis*. 2005;22:319-329.
15. Asagiri M, Takayanagi H. The molecular understanding of osteoclast differentiation. *Bone*. 2007;40:251-264.
16. Varin A, Pontikoglou C, Labat E, Deschaseaux F, Sensebe L. CD200R/CD200 inhibits osteoclastogenesis: new mechanism of osteoclast control by mesenchymal stem cells in human. *PLoS One*. 2013;8:e72831.
17. Garbe AI, Roscher A, Schuler C, et al. Regulation of bone mass and osteoclast function depend on the F-actin modulator SWAP-70. *J Bone Miner Res*. 2012;27:2085-2096.
18. Grigoriadis AE, Kennedy M, Bozec A, et al. Directed differentiation of hematopoietic precursors and functional osteoclasts from human ES and iPS cells. *Blood*. 2010;115:2769-2776.
19. Feng S, Deng L, Chen W, Shao J, Xu G, Li YP. Atp6v1c1 is an essential component of the osteoclast proton pump and in F-actin ring formation in osteoclasts. *Biochem J*. 2009;417:195-203.
20. Liu Y, Wang C, Wang G, et al. Loureirin B suppresses RANKL-induced osteoclastogenesis and ovariectomized osteoporosis via attenuating NFATc1 and ROS activities. *Theranostics*. 2019;9:4648-4662.
21. Zhao H, Feng J, Seidel K, et al. Secretion of shh by a neurovascular bundle niche supports mesenchymal stem cell homeostasis in the adult mouse incisor. *Cell Stem Cell*. 2014;14:160-173.
22. Li J, Xu J, Cui Y, et al. Mesenchymal sufu regulates development of mandibular molars via Shh signaling. *J Dent Res*. 2019;98:1348-1356.
23. Bissey PA, Mathot P, Guix C, et al. Blocking SHH/patched interaction triggers tumor growth inhibition through patched-induced apoptosis. *Cancer Res*. 2020;80:1970-1980.
24. Guo Y, Yuan Y, Wu L, et al. BMP-IHH-mediated interplay between mesenchymal stem cells and osteoclasts supports calvarial bone homeostasis and repair. *Bone Res*. 2018;6:30.
25. Scales SJ, de Sauvage FJ. Mechanisms of Hedgehog pathway activation in cancer and implications for therapy. *Trends Pharmacol Sci*. 2009;30:303-312.
26. Warnakulasuriya S. Global epidemiology of oral and oropharyngeal cancer. *Oral Oncol*. 2009;45:309-316.
27. Laraway DC, Lakshmiah R, Lowe D, Roe B, Rogers SN. Quality of life in older people with oral cancer. *Br J Oral Maxillofac Surg*. 2012;50:715-720.
28. Jimi E, Furuta H, Matsuo K, Tominaga K, Takahashi T, Nakanishi O. The cellular and molecular mechanisms of bone invasion by oral squamous cell carcinoma. *Oral Dis*. 2011;17:462-468.
29. Das S, Samant RS, Shevde LA. The hedgehog pathway conditions the bone microenvironment for osteolytic metastasis of breast cancer. *Int J Breast Cancer*. 2012;2012:298623.
30. Teixeira LN, de Castro RL, Alonso GC, Coletta RD, Rosa AL, de Oliveira PT. Osteopontin expression in co-cultures of human squamous cell carcinoma-derived cells and osteoblastic cells and its effects on the neoplastic cell phenotype and osteoclastic activation. *Tumour Biol*. 2016;37:12371-12385.
31. Zhang X, Junior CR, Liu M, Li F, D'Silva NJ, Kirkwood KL. Oral squamous carcinoma cells secrete RANKL directly supporting osteolytic bone loss. *Oral Oncol*. 2013;49:119-128.
32. Shibahara T, Nomura T, Cui NH, Noma H. A study of osteoclast-related cytokines in mandibular invasion by squamous cell carcinoma. *Int J Oral Maxillofac Surg*. 2005;34:789-793.
33. Okamoto M, Hiura K, Ohe G, et al. Mechanism for bone invasion of oral cancer cells mediated by interleukin-6 in vitro and in vivo. *Cancer-Am Cancer Soc*. 2000;89:1966-1975.

34. Takayama Y, Mori T, Nomura T, Shibahara T, Sakamoto M. Parathyroid-related protein plays a critical role in bone invasion by oral squamous cell carcinoma. *Int J Oncol*. 2010;36:1387-1394.
35. Tang CH, Chuang JY, Fong YC, Maa MC, Way TD, Hung CH. Bone-derived SDF-1 stimulates IL-6 release via CXCR4, ERK and NF-kappaB pathways and promotes osteoclastogenesis in human oral cancer cells. *Carcinogenesis*. 2008;29:1483-1492.
36. Kayamori K, Sakamoto K, Nakashima T, et al. Roles of interleukin-6 and parathyroid hormone-related peptide in osteoclast formation associated with oral cancers: significance of interleukin-6 synthesized by stromal cells in response to cancer cells. *Am J Pathol*. 2010;176:968-980.
37. Mundy GR. Metastasis to bone: causes, consequences and therapeutic opportunities. *Nat Rev Cancer*. 2002;2:584-593.
38. Papadimitrakopoulou VA, Brown EN, Liu DD, et al. The prognostic role of loss of insulin-like growth factor-binding protein-3 expression in head and neck carcinogenesis. *Cancer Lett*. 2006;239:136-143.
39. Goda T, Shimo T, Yoshihama Y, et al. Bone destruction by invading oral squamous carcinoma cells mediated by the transforming growth factor-beta signalling pathway. *Anticancer Res*. 2010;30:2615-2623.
40. Hankenson KD, Gagne K, Shaughnessy M. Extracellular signaling molecules to promote fracture healing and bone regeneration. *Adv Drug Deliv Rev*. 2015;94:3-12.
41. Zhou X, Temam S, Oh M, et al. Global expression-based classification of lymph node metastasis and extracapsular spread of oral tongue squamous cell carcinoma. *Neoplasia*. 2006;8:925-932.
42. Kim EJ, Lee MJ, Li L, Yoon KS, Kim KS, Jung HS. Failure of tooth formation mediated by miR-135a overexpression via BMP signaling. *J Dent Res*. 2014;93:571-575.
43. Ihle CL, Straign DM, Provera MD, Novitskiy SV, Owens P. Loss of myeloid BMPR1a alters differentiation and reduces mouse prostate cancer growth. *Front Oncol*. 2020;10:357.
44. Pickup MW, Hover LD, Guo Y, et al. Deletion of the BMP receptor BMPR1a impairs mammary tumor formation and metastasis. *Oncotarget*. 2015;6:22890-22904.
45. Singh A, Sweeney MF, Yu M, et al. TAK1 inhibition promotes apoptosis in KRAS-dependent colon cancers. *Cell*. 2012;148:639-650.
46. Gooding S, Olechnowicz S, Morris EV, et al. Transcriptomic profiling of the myeloma bone-lining niche reveals BMP signalling inhibition to improve bone disease. *Nat Commun*. 2019;10:4533.
47. Choi JY, Lee YS, Shim DM, Seo SW. PTCH1 regulates anchorage-independent growth and bone invasion of non-small cell lung cancer cells. *Bone*. 2021;144:115829.
48. Nishimori H, Ehata S, Suzuki HI, Katsuno Y, Miyazono K. Prostate cancer cells and bone stromal cells mutually interact with each other through bone morphogenetic protein-mediated signals. *J Biol Chem*. 2012;287:20037-20046.

SUPPORTING INFORMATION

Additional supporting information may be found in the online version of the article at the publisher's website.

How to cite this article: Qiao Q, Xu L, Li Q, et al. Bone morphogenetic protein receptor 1α promotes osteolytic lesion of oral squamous cell carcinoma by SHH-dependent osteoclastogenesis. *Cancer Sci*. 2022;113:1639–1651. doi:10.1111/cas.15330